Egyptian Journal of Physics Science

Significance of Lanthanum Doping on Physical, Optical, Magnetic, and Dielectric Properties of $CoAl_{2-x}La_xO_4$ Nanoparticles

Abdel-Hamed A. Sakr[*]

[*]*Physics Department, Faculty of Science, Damanhur University, Damanhur, Egypt.*

IN the present work, the effects of La^{3+} substitution on structural, optical, dielectric, and magnetic properties of cobalt aluminates nanoparticles were investigated. ($CoAl_{2-x}La_xO_4$), in series $0.0 \leq x \leq 0.12$, nanoparticles were successfully synthesized via co-precipitation method. X-ray powder diffraction was employed to verify the cubic spinel aluminate structure. Lattice parameter (*a*) was increased from 8.078 to 9.983 and X-ray density ($r_{x\text{-}ray}$) of the structure was increased from 4.489 to 4.532 with increasing the La^{3+} content. Transmission electron microscopy analysis showed homogenous formation of the nanoparticles in a spherical shape, while functional analysis via FTIR indicated the presence of two main absorption attributed to the spinel aluminate. Optical properties of cobalt aluminates nanoparticles were investigated from results of optical absorbance spectra. Moreover, the increase in La^{3+} content, is followed by an increase from 1.01eV to 1.60 eV in the optical energy gap E_{opt} and from 2.930 to 4.983 in the refractive index. This confirms the enhancement of density of the $CoAl_2O_4$ nanoparticles with rising La^{3+} content. Results show an increase in the ferromagnetic behavior (superparamagnetic) with addition of La^{+3} content which may be due to the formation of single domain particle of small particle size. The saturation magnetization increases from 0.736 to 2.314 emug^{-1} as the contents of La^{3+} increases in the spinal $CoAl_2O_4$. The impedance, dielectric constant, dielectric loss and loss tangent (tan δ) were found to be changed and improved with rising La^{3+} content.

Keywords: Spinel aluminate, cobalt aluminates nanoparticles, dielectric properties, La^{3+} substitution.

Introduction

For multiple optoelectronic and photonic device applications, Perovskite materials (PM) have recently emerged as a promising and effective low-cost energy materials [1].The PM durability is due to the thermal and chemical stability [2]. These spinel aluminates nanoparticles have attracted much attention among nanomaterials because of its convenient for a wide range of applications including catalysis, ceramics, magnetic materials [3], and humidity sensor [4]. Spinels are a category of binary metal oxides having the general structural formula AB_2O_4, where A^{II} = a divalent cation such as Co, Ni, Mg, Cr, Mn, Cu, Fe, Zn etc. and B^{III} = a trivalent cation like In, Al, Ga, Ti etc. [2-4]. AB_2O_4 is the formula of Normal spinels where the divalent A cations occupy the tetrahedral sites and the trivalent B cations occupy the octahedral sites in a close-packed arrangement of oxide ions. A normal spinel can be represented as $(A^{II})^{tet}(B^{III})_2^{oct}O_4$ and oxygen has fcc close packing arrangement [2-5]. Among the spinel aluminates, cobalt aluminate ($CoAl_2O_4$) is widely used as catalyst and color filter; it has good ultraviolet and visible light opacity, chemically inert, heat resistant, and stable to ultraviolet light [4–6].

The properties of nanomaterials depend on the composition, size, shape, size distribution, and preparation technique [7–11]. For

preparation of nano oxides, several techniques were used including sol-gel [12,13], ball milling, hydrothermally [14], and co-precipitation [15], which is the widely used technique in preparation of nano-crystalline due to its low cost and simplicity [8]. Both optical and magnetic properties of the nano-crystalline aluminates are highly dependable on distribution of cations between the A– and B– sites of the spinel structure. Several previous studies analyzed and tracked the effect of cations substitution in order to improve the dielectric, optical, electrical and magnetic properties of spinel aluminates [16-19].

This study focused on the effect of La^{3+} substitution on structural, morphological, magnetic, optical, and dielectric properties of $CoAl_{2-x}La_xO_4$ ($0.00 \leq x \leq 0.12$). Nano aluminates that were synthesized by co-precipitation method were characterized by X-ray powder diffraction (XRD), Fourier transform infrared (FTIR), transmission electron microscope (TEM), Digital dielectric bridge (LCR), and vibrating sample magnetometer (VSM). Moreover, the optical and dielectric parameters have been also calculated and investigated.

Experimental Procedures

Co-precipitation method was employed in order to prepare $CoAl_{2-x}La_xO_4$ nanoparticles, with different La contents ($0.00 \leq x \leq 0.12$.) Stoichiometric amounts of $CoC_{l2}.6H_2O$, $LaCl_3.6H_2O$ and $AlCl_3.6H_2O$ were obtained. Then, aqueous solutions of the above-mentioned chlorides were prepared. Continuous warming and mixing were carried out until the temperature reached 40 °C. At this point, 0.2 g of Poly(vinyl alcohol), known as PVA, dissolved in 20 ml of distilled water was added which disabled agglomeration of particles. Here, a precipitate is formed as soon as the NaOH solution is added. It is worth mentioning that NaOH solution is added dropwise with continuous stirring till pH of the solution escalated to 12. Simultaneous heating and stirring were done until finishing the addition of NaOH and till the temperature reached 60°C. Maintaining this temperature (60 °C), we continued to stir for 2 hr. The precipitates are carefully washed with distilled water several times to ensure the removal of unwanted salt residues as well as the excess of NaOH making sure the precipitate becomes neutral (PH = 7). Once we reach this point in the experiment, the precipitate is dried to get rid of any remaining water contents. For 4 hr, the dried powder is calcined at 600 °C to obtain the nano-powder and to refine the crystalline properties.

The XRD for $CoAl_{2-x}La_xO_4$ nanoparticles was done in a Brucker-AXS D8 were advance powder diffractometer. Jeol transmission electron microscope (JEM- 2100-Jaban) was used to check the particle morphology. Using FTIR 8400S Shimadzu spectrophotometer, FTIR spectrum was recorded. The magnetic properties of $CoAl_{2-x}La_xO_4$ nanoparticles ($0.00 \leq x \leq 0.12$) were investigated by the vibrating sample magnetometer (VSM) (Lakeshore 7410). The dielectric properties of $CoAl_{2-x}La_xO_4$ nanoparticles were measured using the Digital LCR Meter (Hioki 3532–50) at 50 kHz to 5 MHz range.

Results and Discussion

X-ray diffraction

The XRD spectrum of $CoAl_{2-x}La_xO_4$ for a range between $0.00 \leq x \leq 0.12$ nano-crystals are shown in Fig.1. All diffraction peaks that appeared indicate cobalt aluminate formation with the spinel cubic structure (JCPDS number 44-016) [19, 20]. This suggests the replacement of Al^{3+} ion by La^{3+} in $CoAl_2O_4$ sample, [20, 21]. The important evidence of formation spinel phase can be assured by the incipient presence of (311) plane situated at $2\theta = 37.2°$, and it can also be confirmed by the visual observation of the blue color that distinguishes cobalt aluminum. The intensities of the (220) and (440) planes are more sensitive to the cations on tetrahedral, and octahedral, respectively [20]. Indeed, the Co^{2+} and Al^{3+} ions have a strong preference to occupy A and B sites, respectively [21]. The diffraction peaks at $2\theta = 31.12°$ and $33.11°$, which were indexed as $LaAlO_3$ for series with $x \geq 0.10$ and implied that no more La cations could be accommodated in $CoAl_2O_4$. In addition, weak diffraction peaks were observed when the La doped series have been compared to the undoped $CoAl_2O_4$. The crystallinity degree of the cubic spinel aluminates could be assessed by main diffraction peak intensity at 311 plane. In addition, sample crystallization becomes more difficult with amorphous-like phases starting to appear by the gradual increase of La^{3+} content, as shown in Figure 1. This could be related to the high potential barrier of La^{3+} ion that is required to enter the spinel crystal lattice when increasing the dopant concentration. Additionally, the XRD peaks started to be weak and wide for the series with $x = 0.10$ and 0.12, which suggests a decrease in the crystallinity and crystallite size.
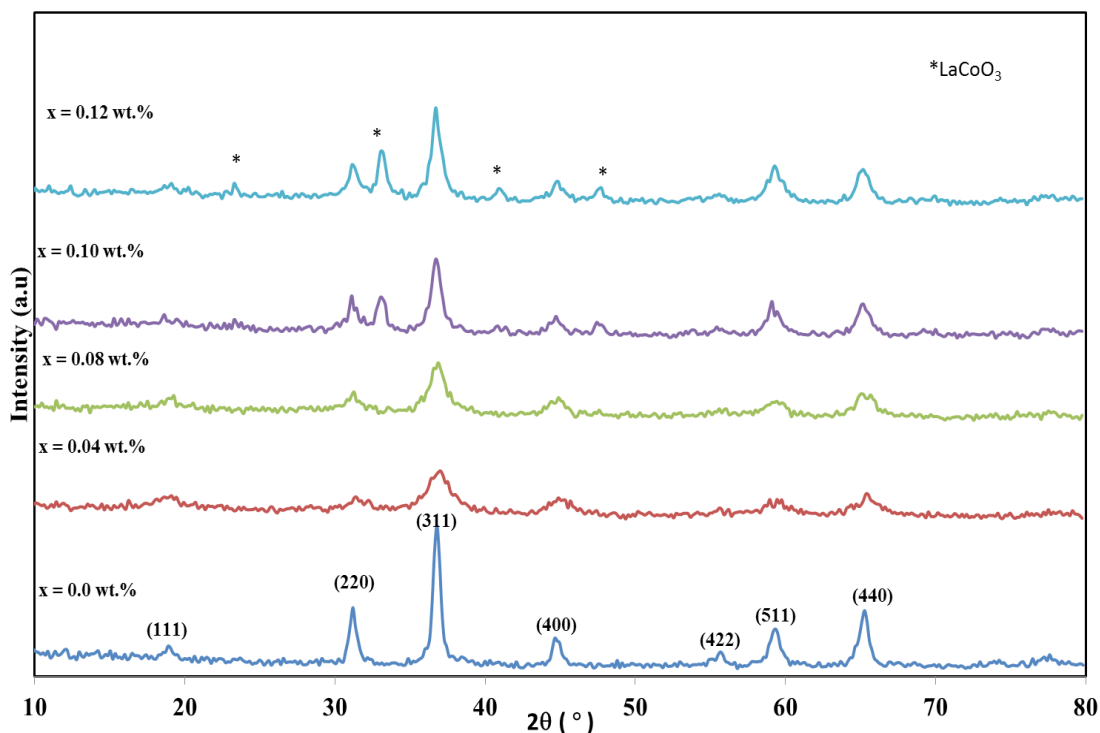
Fig. 1. X- ray diffraction patterns of CoAl$_{2-x}$La$_x$O$_4$ nanoparticles (0.00 ≤ x≤ 0.12) annealed at 600 ºC .

The lattice parameter a = 8.059 Å   for undoped cobalt aluminates nanoparticles sample which are reported in Table 1, in agreement with that reported in the JCPDS card [21], and the value was increased to 8.109 Å by increasing La^{3+}content. The relationship between Lattice parameter a with lanthanum content was almost largely linear dependence since as lanthanum content increases, Lattice parameter a increases as shown in Fig. 2, and this obeys Vegard's law [22], which indicates the formation of a homogeneous solid solution in all   CoAl$_{2-x}$La$_x$O$_4$ (0.0 ≤ x ≤ 0.12) matrices annealed at 600 ºC. There was a decrease in magnetic ions release by increasing lattice parameter due to the increased content of lanthanum, due to the larger ionic radius of La^{3+}(0.615 Å) compared to that of Al^{3+}(0.53 Å). Such increased radius separates between the magnetic ions, causes an increased hopping length, or La^{3+}cations might enter into the octahedral sites replacing the Al^{3+} cations, which could expand the unit cell [22]. It is observed that the X-ray density (d_xr$_{XRD}$) was increased with an increase of lanthanum concentration, which in turns increased the molecular weight (M_wM$_w$) and that suppressed the increase of the lattice

constant values. Both the strain ε and the average crystallite size (D) of the prominent peak at 311 reflection in accordance with modified Debye-Scherrer formula [21,22, 23].

Results in Figure 3 showed the plot of $\beta \cos\theta$ versus $4\sin\theta$ of CoAl$_{2-x}$La$_x$O$_4$ nanoparticles at x = 0.00, 0.04, 0.08, 0.1 and 0.12. Both the strain ⧠ and the crystalline size were obtained from the slope and the intercept, respectively. The crystallite size was gradually decreased with the increase in La^{3+} content (Table 1-a).

The distance between magnetic ions, (L$_a$ for tetrahedral (A) site and L$_b$ for octahedral (B) site) is known as length of jump/hopping 'L'.

Theoretical density obtained from X-ray diffraction data d_xr$_{XRD}$, the specific surface area of the particles (S), which is the summation of the areas of the exposed surfaces of the particles per unit mass, bond lengths R$_A$ and R$_B$, The oxygen positional parameter (U$_o$) and the polaron radius (r$_p$) for all CoAl$_{2-x}$La$_x$O$_4$ nanoparticles samples are calculated using the following relations [24,25, 26] :

$$l_a = \frac{a_{exp}\sqrt{3}}{4} \qquad \text{and} \qquad l_b = \frac{a_{exp}\sqrt{2}}{4}$$

1-a

$$\rho_{XRD} = \frac{8M}{N\ a_{exp}^3}$$

1-b

$$S = \frac{6}{D\ \rho_{XRD}}$$

1-c

$$R_A = \frac{(u-1/4)}{4}a\sqrt{3} - r_o \qquad \text{and} \qquad R_B = (5/8-u)a - r_o$$

1-d

$$U_o = \frac{\frac{1}{4}R^2 - \frac{2}{3} + \left[\frac{11}{48}R^2 - \frac{1}{18}\right]^{1/2}}{2R^2 - 2}$$

1-e

$$r_p = \frac{1}{2}\left[\frac{\pi}{6N'}\right]^{\frac{1}{3}}$$

1-f

where a_{exp} is experimental Lattice parameter , M is the molecular weight expressed in grams, (a) is the lattice constant and N is Avogadro's number (6.023 x 10^{23} molecule / mole). (D) Scherrer's grain diameter of the spinel powders, R_B, R_A are average bond lengths, $R = R_B/R_A$ and N' number of sites per unit volume $=96/a^3$

As seen from Table 1.b the Probability of electron hopping between B and B sites is much more occurrence than A and B sites, since the values L_a , is greater than that L_b [27,28], This was evident from the values of Bond lengths R_B which more than the values of Bond lengths R_A. Using the experimental va l u e s of lattice parameter a, oxygen positional parameter u was calculated (u=0.371 Å). The charge carriers are not completely free but are s t r o ngly localized may be due to formation of polarons, the values of polaron radius increased with increased of La^{3+} content.
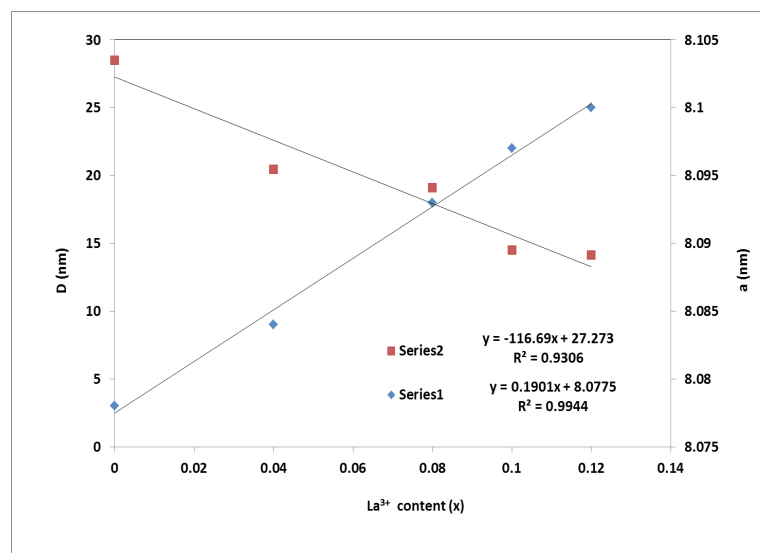

Fig. 2. The dependence of crystallite size (*D*) from Sherrer and lattice parameter (a) on lanthanum (La³⁺) content for CoAl₂₋ₓLaₓO₄ nanoparticles.
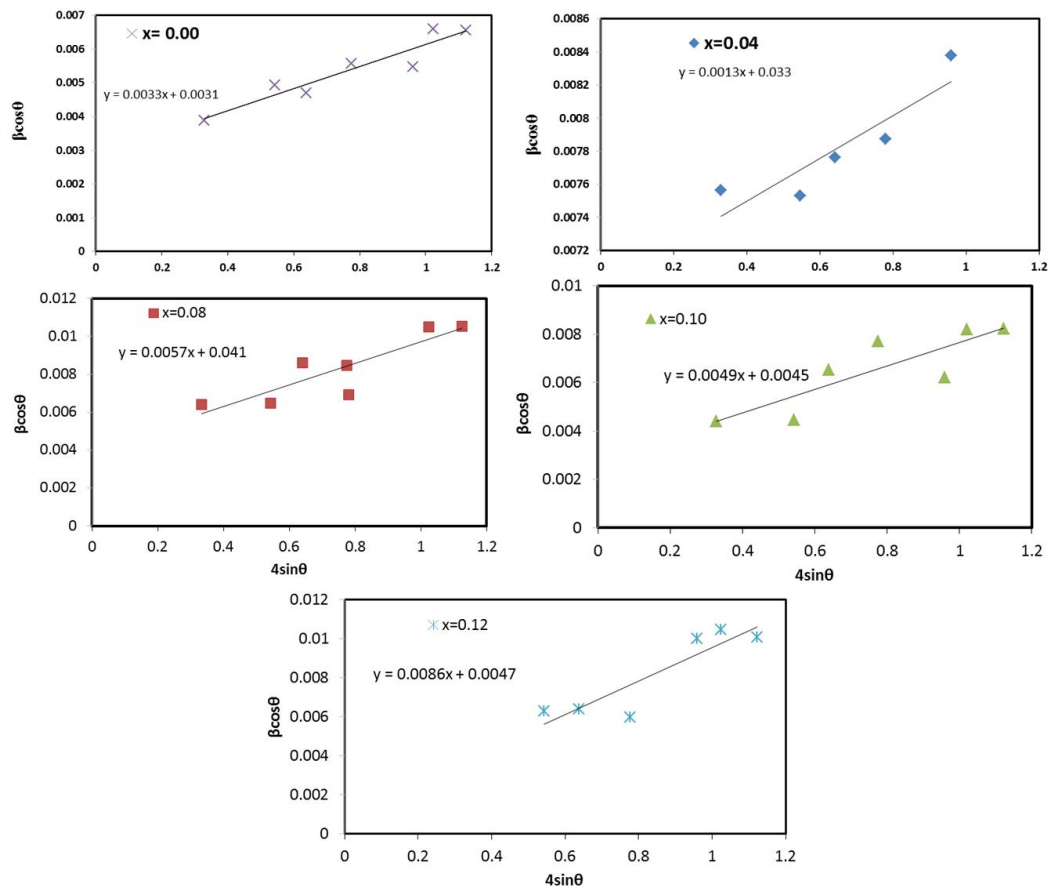
Fig. 3. Plot of $\beta \cos \theta$ Vs. $4 \sin \theta$ for different La3+contents, x=0.00, 0.04, 0,08, 0.10 and 0.12.

TABLE 1.a . lattice parameter (a) (a), average crystallite sizes (D) of CoAl$_{2-x}$La$_x$O$_4$ nanoparticles $(0.00 \leq x \leq 0.12)$.

X	Lattice constant	Scherrer equation	Williamsone Hall method		TEM
	(a) (nm)	D (nm)	D (nm)	$\mathcal{E} \times 10^{-2}$	D (nm)
0.0	80.78	28.50	44.73	0.33	58.42
0.04	80.84	20.46	42.02	0.13	44.31
0.08	80.93	19.102	33.82	0.57	14.21
0.10	80.97	14.50	25.21	0.49	13.18
0.12	81.00	14.13	24.33	0.86	13.45

TABLE 1.b. A-site jump length (L$_a$) , B-site jump length (L$_b$), X-ray density (d_xr$_{x-ray}$) and Bond lengths (RA, RB), and oxygen position parameter (u$_o$) of CoAl$_{2-x}$La$_x$O$_4$ nanoparticles (0.00 ≤ x≤ 0.12) .

X	L$_a$ (Å)	L$_b$ (Å)	d_x $_{x-ray}$ (g/cm^3)	R$_A$(Å)	R$_B$ (Å)	S (m²/g)	r$_p$ (Å)
0.0	3.498	2.856	4.489	1.611	1.882	46.898	0.7108
0.04	3.500	2.858	4.491	1.612	1.883	65.298	0.7113
0.08	3.504	2.861	4.501	1.614	1.885	69.785	0.7121
0.10	3.506	2.863	4.519	1.615	1.886	91.567	0.7125
0.12	3.507	2.864	4.532	1.616	1.887	93.696	0.7127

Morphology of nanoparticles using TEM

TEM Results showed the structure morphology for CoAl$_{2-x}$La$_x$O$_4$at x= 0.00, 0.04, 0.1 and 0.12 as shown in Fig. 4a, 4b, 4c and 4d, respectively. TEM images revealed that the nanoparticles were approximately homogeneous in shape and size with pseudo-particles and spherical nanoparticles. Agglomerated nanoparticles are observed due to present of magnetic interactions between nanoparticles and heating the powder at 600 °C in air. Moreover, the degree of agglomeration was increased for higher additive of La^{3+} content which can attribute to increase in the strength of magnetic interactions among nanoparticles. The average grain size values are tabulated in Table 1-a . The current results from TEM were consistent with the results obtained from XRD measurements.

Fourier Transform Infrared (FTIR) Analysis

FT-IR spectra of the as-synthesized CoAl$_{2-x}$La$_x$O$_4$ (0.00 ≤ x ≤ 0.12) nanoparticles in the range of 300–4000 cm^{-1} (Figure 5) is essential to describe both ion vibration mode and deformation of the spinel structure. FTIR spectra would explain the nature and strength of chemical bonds that can be formed or disappear in prepared samples as a result of addition of La^{3+} content. were recorded. It was reported that the formation of spinel aluminates was confirmed by the existence of the main absorption band υ$_1$ and ʊ$_2$, in the wavelength wavenumber ranged from 550 to 700 cm^{-1} in all samples [26].

The highest band υ$_1$, observed around 660 cm^{-1}, that could be attributed to intrinsic stretching vibrations of metal at the tetrahedral site, whereas the υ$_2$ lowest band, observed around 550 cm^{-1} , which may be corresponded to octahedral- metal stretching. The υ$_1$ and υ$_2$ bands are due to Al^{3+} - O^{2-} complexes present at A and B-sites as a result of the formation of aluminate spinel. The Co^{2+} ions occupy mainly the octahedral sites and fraction goes into tetrahedral sites [27,28]. Change in the La^{+3} content effected the intensities and positions of the absorption bands υ$_1$ and υ$_2$

However, the broad bands appeared around 3450 and 1640 cm^{-1} could be a result of hydrogen bonding O–H [27]. The common band appeared at around 2426 cm^{-1} might be resulted from passing the IR beam through air [28]

It was observed that the position of bands for the substituted samples were shifted to lower values of wavenumber in respect to the observed samples for the as-prepared sample (Fig. 5). This might be attributed to the presence of La^{3+} cations on the octahedral (B) sites because of its higher atomic weight and larger ionic radius than Al^{3+} cations, which might have an effect on Al^{3+}– O^{2-} distances on B-sites.

UV-Vis Spectroscopy

UV-vis spectra from CoAl$_{2-x}$La$_x$O$_4$ nanoparticles were recorded using a UV–visible spectrophotometer (Fig. 6-a). An absorption band were observed around 200nm in the ultraviolet (UV) area and a strong two absorption peak at 450 and 680 nm, which confirmed the existence of tetrahedral Co^{2+} cations in the CoAl$_2$O$_4$ spinel [1,5].
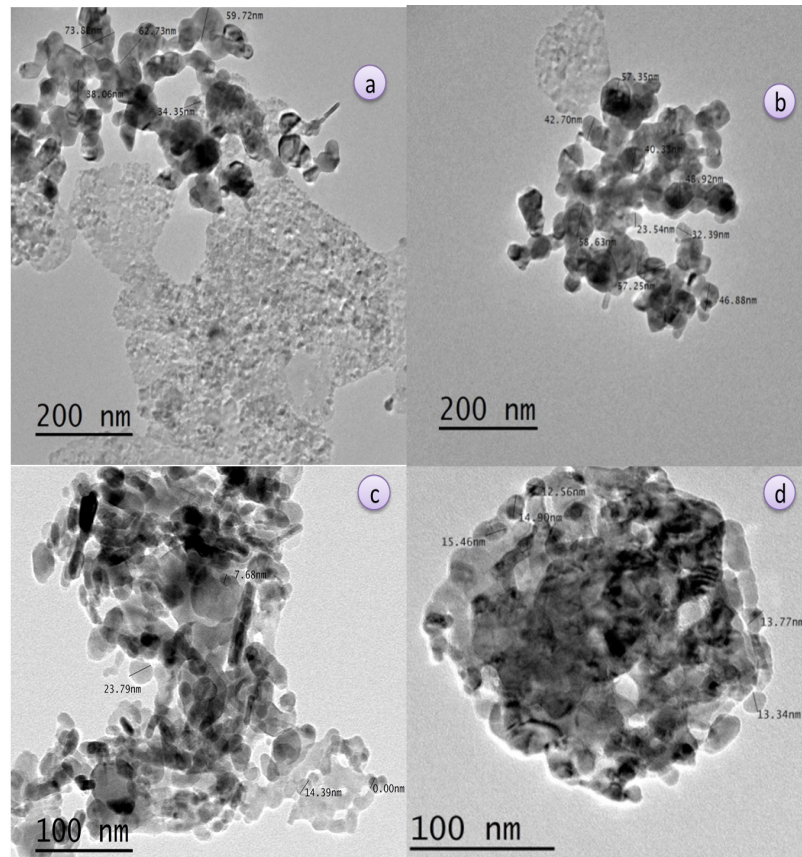
Fig. 4. TEM for CoAl$_{2-x}$La$_x$O$_4$ nanoparticles, (a) X= 0.00, (b) X= 0.04, (c) X= 0.10 and (d) X= 0.12.

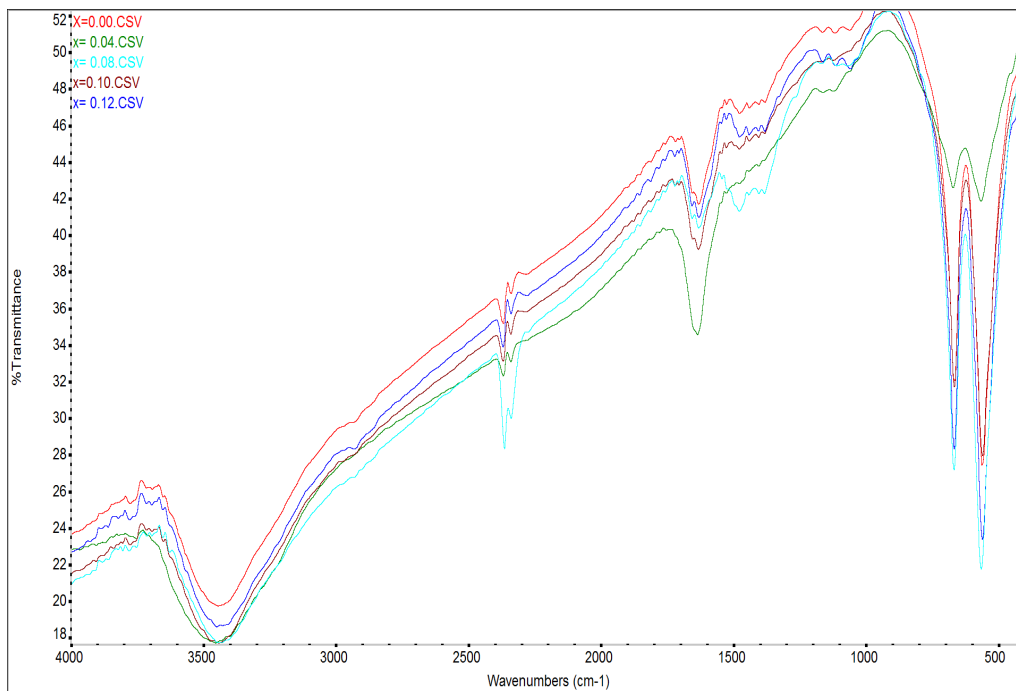**Fig. 5. FT-IR pattern of as-synthesized CoAl$_{2-x}$La$_x$O$_4$ nanoparticles with different   La^{3+} content (0.00 ≤ x ≤ 0.12), annealed at 600 ºC.**

The blue shift in the absorption band edge wavelength λ_g (nm) might be affected by the crystallite and the particle size [27]. The change in the coordination state of Co^{2+} ion (from octahedral to tetrahedral) resulted in the observed shift in the absorption peak. The absorption coefficient a, which is proportional to the Kubelka–Munk function is given by [27].

$$\alpha(\omega) \approx \mathrm{h}\ F(R) = \mathrm{h}\ \alpha_0 + \frac{\hbar\omega}{\Delta E_u} \qquad \text{(2-a)}$$

where $F(R) = \frac{(1-R)^2}{2R}$, R is reflectance (%), α_0 is constant and ΔE_u is the width of the band tail of localized states in the normally forbidden band gap (Urbach energy). According to the Tauc's relation [28], the absorption coefficient near the fundamental edge can be calculated according to the following equation.

$$\alpha\hbar\omega = B\left(\hbar\omega - E_g\right)^m \qquad \text{(2-b)}$$

where B is an energy-independent constant, E_g is the optical band gap energy, h is the Planck's constant, $w=2pn$ where n is the frequency of the incident photon, where n is an index determined by the nature of the electron transition during the absorption process, m may have values 1/2, 3/2, 2 and 3 for direct allowed (E^d_{opt}), direct forbidden , indirect allowed (E^i_{opt}) and indirect forbidden respectively. The absorption peak shifts towards the blue region as the coordination geometries of Co^{2+} ion changed from the octahedral to the tetrahedral coordination.

As shown in Figures 6 (a), 6(b), 6(c) and 6 (d) the absorption band edge wavelength λ_g, Urbach energy ΔE_u, direct (E^d_{opt}), and indirect (E^i_{opt}) optical band gap energies can be calculated and listed in Table 2. Urbach energy ΔE_u, decreases with increasing La^{3+} content, this is may be due the decrease in the width of localized states in the optical band. The increase in optical energy band gap could be because of the decrease of the particle size and the decrease of density of localized state in the conduction band [27,29].
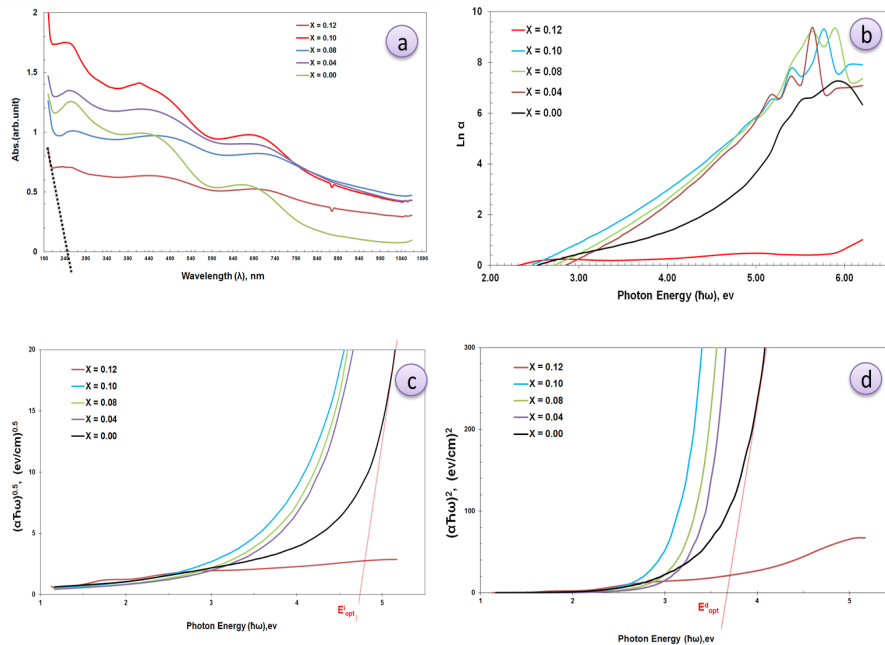

Fig. 6. Optical properties of CoAl$_{2-x}$La$_x$O$_4$ (a) UV–Vis spectra, (b) Urbach plots, (c) Plots of ($\alpha h\omega$)^2 vs. $h\omega$ and (d) Plots of ($\alpha h\omega$)$^{0.5}$ vs. $h\omega$.

The refractive index n can be determined from the optical band gap (E_{opt}) according to the empirical relation

$$\frac{n^2 - 1}{n^2 + 2} = 1 - \sqrt{\frac{E_{opt}}{\emptyset}} \quad (3)$$

As shown in Table 2, the increase La^{3+} content, the increase the refractive index values which confirms the enhancement of density of the CoAl$_2$O$_4$ nanoparticles with rising La^{3+} content

Magnetic Measurement

For accurate study and understanding, the effect of the size of CoAl$_{2-x}$La$_x$O$_4$ nanoparticles, on the magnetic properties, magnetization measurements were carried out on a vibrating sample magnetometer with a maximum applied field of ±20 kG at room temperature. As shown in magnetic hysteresis (*M – H)* curves in Fig. 7. From these curves, the saturation magnetization (M$_s$), coercivity field (H$_c$), squareness ratio (S) and the magnetic moment (μ$_m$) and remanence magnetization (M$_r$) were obtained and were given in Table 3. For undoped sample, a small hysteresis was observed indicating a weak ferromagnetic nature of the material, due to the formation of a single ferromagnetic domain which is preferred in smaller particles. Moreover, a stable bulk magnetization cannot be established due to thermal fluctuations acting on small particles and consequently the system exhibits super paramagnetism [30].

TABLE 2. Absorption band edge wavelength λ$_g$ (nm), direct, indirect optical band gap and Urbach energy ΔE$_u$ of CoAl$_{2-x}$La$_x$O$_4$ nanoparticles.

X	lg(eV)	E^d_{opt} (eV)	E^i_{opt} (eV)	ΔE$_u$ (eV)	n
0.0	285	3.85	1.60	1.024	2.934
0.04	282	3.60	1.41	0.976	3.049
0.08	258	3.25	1.25	0.587	4.983
0.10	240	3.90	1.46	0.553	2.577
0.12	232	3.35	1.01	0.724	3.369

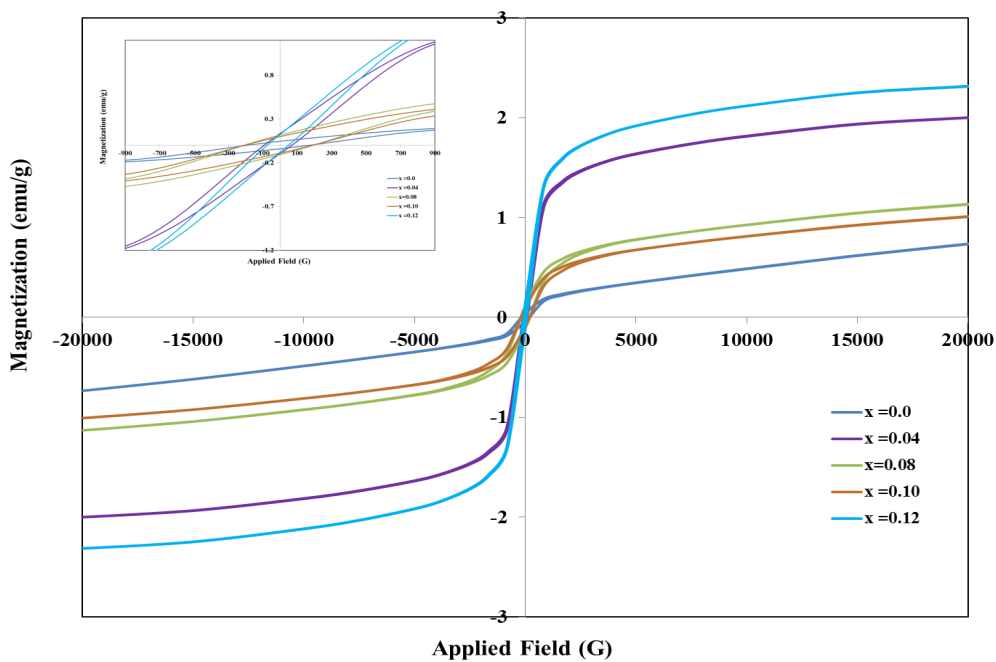**Fig. 7. M-H curves of CoAl$_{2-x}$La$_x$O$_4$ nanoparticles .**

TABLE 3. Saturation magnetization (M_s), coercivity field (H_c), squareness ratio (S) , remanence magnetization (M_r) anisotropy constant (k), and magnetic moment (μ_m) for $CoAl_{2-x}La_xO_4$ nanoparticles, $(0.00 \leq x \leq 0.12)$.

x	Ms (emu/g)	$M_r \times 10^{-2}$ (emu/g)	Squareness ratio	H_c (G)	Anisotropy parameter K	μ_m
0	0.736	4.30	0.058	174.64	128.472	0.023
0.04	2.000	11. 50	0.057	78.464	156.959	0.064
0.08	1.132	11.20	0.099	197.36	223.490	0.036
0.1	1.010	9.49	0.093	193.37	195.245	0.033
0.12	2.314	10. 20	0.044	60.483	139.969	0.076

The ferromagnetic behavior of nanocrystalline sample is due to change of cation distribution with decrease of particle size which leads to a reduction in ligand field strength [30, 31]. If all divalent cations occupy all the tetrahedral sites, then the material is a normal spinel. If all the divalent cations occupy all the octahedral sites, then it is an inverted spinel and if the divalent cations are distributed among both the tetrahedral and octahedral sites, the material is a partially inverted spinel. Therefore, in $CoAl_{2-x}La_xO_4$ nanoparticles, some of Li^{3+} cations occupy the tetrahedral (A) sites, which switch on the A–B superexchange interaction and give rise to a ferromagnetic behavior.

From Table 3, we can observe that the saturation magnetization increases from 0.736 to 2.314 emug^{-1} as the contents of La^{3+} increases in the spinal $CoAl_2O_4$. This may be due to the zero magnetic moment of Al^{3+} cations which are partially replaced by the larger magnetic moment of La^{3+} cations (4.0 µB) in the octahedral site [30]. The magnetic moment (μ_m) per unit formula in Bohr magneton was calculated from saturation magnetization by using the following formula :

$$\mu_m = \frac{M_W X M_s}{5585} \tag{4}$$

Where: μ_m is the magnetic moment, M_W is the molecular weight, M_s is the Saturation magnetization and the factor 5585 is a magnetic factor.

The deviation of squareness ratio S in $CoAl_{2-x}La_xO_4$ nanoparticles from typical single domain isolated ferromagnetic particles (S ~1) may be Construed to the interactions among grains, which are affected by core-shell structure of grains and grain size distribution in the material. Both the particle size and crystal morphology have important effects on the magnetic property [30, 31].

Dielectric properties

The dielectric properties of $CoAl_{2-x}La_xO_4$ nanoparticles are measured in the frequency range of 42 Hz to 5MHz at room temperature. The complex impedance (Z) ,the real (ε'e') and imaginary (e″) parts of dielectric constant, ac conductivity (σ), dielectric loss ($\tan\delta$) and the real M′ and imaginary M″ parts of modulus are calculated using the following relations :

$$Z = Z' - jZ'', \quad Z' = Z\sin\varphi, \quad Z'' = Z\cos\varphi \tag{5-a}$$

$$\varepsilon' = \frac{Z''}{2\pi f |Z|^2 C_o} \quad and \quad \varepsilon'' = \frac{Z'}{2\pi f |Z|^2 C_o}, \tag{5-b}$$

$$M' = \frac{\varepsilon'}{\varepsilon'^2 + \varepsilon''^2} \quad and \quad M'' = \frac{\varepsilon''}{\varepsilon'^2 + \varepsilon''^2} \tag{5-c}$$

$$\varepsilon' = \varepsilon_s - \tau(\varepsilon'\omega) \quad and \quad \varepsilon' = \varepsilon_\infty + (1/\tau)(\varepsilon''/\omega) \tag{5-d, 5-e}$$

$$\tan\delta = \frac{Z'}{Z''} = \frac{\varepsilon'}{\varepsilon''} \tag{5-f}$$

$$\sigma_{ac} = 2\pi f \varepsilon_o \varepsilon' \tan\delta$$

Where $C_o = \varepsilon_o A/d$ is the air capacity, A is cross-sectional area, d is the thickness of the pallet , e_o ε_0 is the permittivity in free space , (ф) is the phase angle , t is the relaxation time , ε_s and ε_∞ are the dielectric constant at very low and very high frequency, respectively .

The real (ε') and the imagine (ε'') parts of relative permittivity in the frequency range of 40 Hz–5 MHz of $CoAl_{2-x}La_xO_4$ nanoparticles at room temperature was shown in Fig. 8 (a) and (b). The value of dielectric constant is higher at lower frequencies and decreases with increasing frequency. This is attributed to the decrease of the permanent dipoles as the frequency increases [31,32].
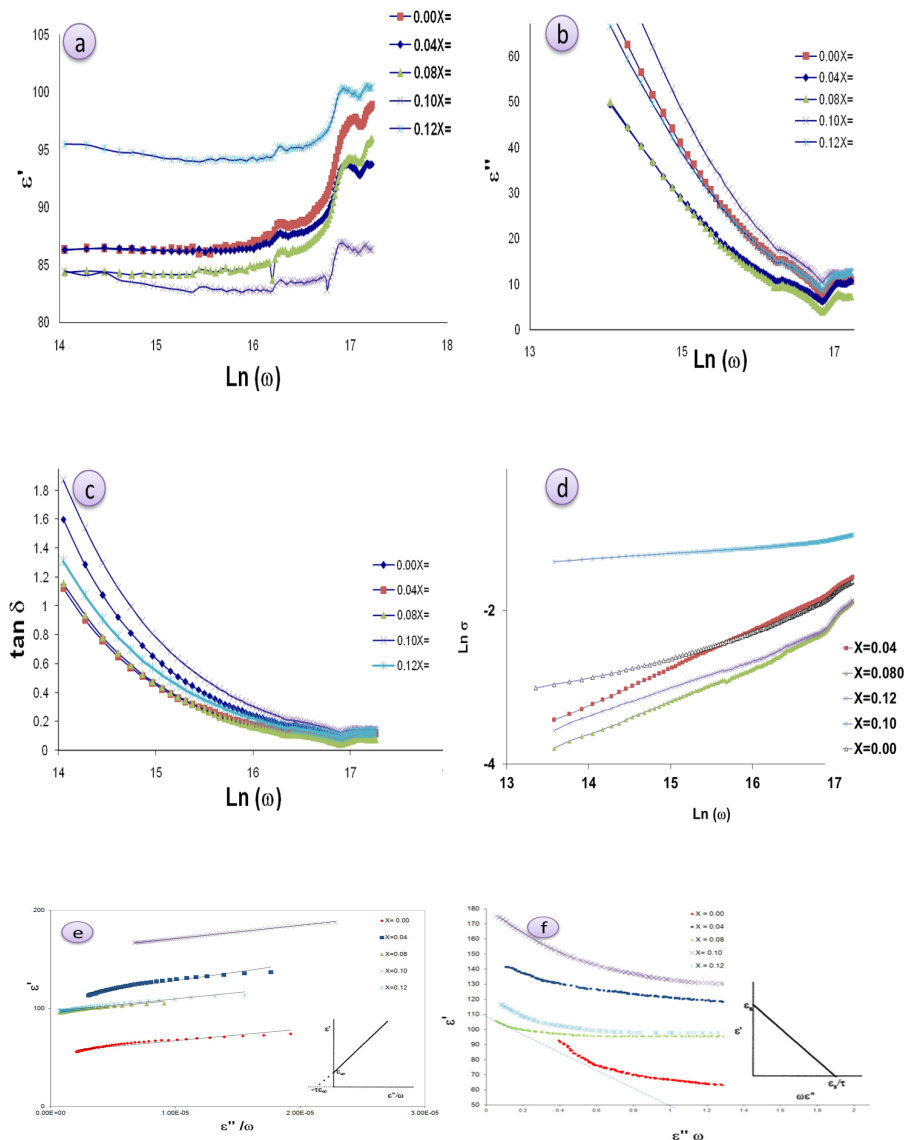

Fig. 8. Variation of (a) ε', (b) ε'', (c) Tan δ, and (d) AC conductivity (σ) with the frequency (in frequency range from 40 Hz to 5 MHz) for $CoAl_{2-x}La_xO_4$ at room temperature. (e)The variation of ε' with (ε''/w). (f) The variation of ε' with (ε''w). *The inset of figures e and f show the calculated ε$_s$, ε$_\infty$, and τ.*

It is clear from Fig. 8 (a), that the values of ε' increases with increasing La^{+3} content in CoAl$_{2-x}$La$_x$O$_4$ nanoparticles. The value of dielectric constant is mainly attributed to an internal barrier layer capacitor (IBLC) model, where grain boundaries act as insulating wall. Meanwhile, another reason is related the decrease in grain size and increasing the surface area of nanoparticles leads to an increase in the number of electric dipoles on the surface which will also contribute to the polarizability of material. Figure 8 (c) shows the variation of tan δ with frequency. It is observed that at lower frequencies the value of tan δ is high and decreased rapidly with the increase in frequency.

The dielectric constant and the dielectric loss are due to the combined effects of: (a) crystal structure perfection, (b) microstructure (porosity), (c) chemical homogeneity and (d) the amount of La^{3+} in the sample. The dominance of each factor varies with the composition of the sample. The dielectric loss arises due to the lag of the polarization behind the applied alternating electric field and is caused by the impurities and imperfections in the crystal lattice [31,32].

As shown in Fig. 8 (d), the total conductivity of a material can be expressed by the relation σ$_{total}$= σ$_o$(T)+σ$_{ac}$(ω, T), where σ$_o$(T) is the frequency independent dc conductivity contributed by band conduction and the σ$_{ac}$ (=Aω^s) is frequency dependent ac conductivity contributed by hopping charge carriers . A is dependent on temperature and indicates the strength of polarizibility and exponent s is the degree of interaction of mobile ions with lattice. The coefficient A and the exponent s are temperature and material intrinsic property dependent [33]. The values are reported in Table 4.

The increase in the value of electrical conductivity with frequency may be due to hopping mechanism [39]. The hopping within ions in B-site increases with frequency. Moreover, the conduction can attribute to the free-charges that released from distinct trapping centers. Thus, increasing in ac-conductivity (σ$_{ac}$) with La^{3+} content (except x= 0.08 and x=0.12) is due to the increasing in grain boundaries at the expense of decreasing in grain size, resulted in the electronic state near to Fermi level is localized. Therefore, the conduction mechanism must become dominated by hopping between localized states. The decrease in the ac conductivity of composites x=0.08 and 0.12 is due to the substitution of Al^{3+} with La^{3+} which increases the concentration of La^{3+} ions at B-site, where the high concentration of La^{3+} ions Reduce and resist the electron hopping causing a decrease in the conductivity.

Figure 8 (e) and (f) show the variation of ε' with (ε"/w) and (ε"w), the values of ε$_s$ and ◻$_◻$ can be calculated and listed in table 4. High dielectric constant and low dielectric loss for the samples x=0.1 and x=0.12 makes these materials good for energy storage at high frequencies such as in supercapacitors. Grain resistance R$_g$, grain capacitance C$_g$, grain boundary resistance R$_{gb}$ and grain boundary capacitance C$_{gb}$ are calculated using the following relations :

5-g

$$\varepsilon_\infty = \frac{1}{c_o} \frac{1}{\frac{1}{C_g}+\frac{1}{C_{gb}}} \quad \text{and} \quad \varepsilon_s = \frac{R^2{}_g\ c_g + R^2{}_{gb}\ c_{gb}}{C_o(R_g + R_{gb})^2}$$

$$\sigma = \frac{1}{C_o(R_g + R_{gb})} \quad \text{and} \quad \tau = \frac{R_g R_{gb}\ (\ c_g + c_{gb}\ )}{(R_g + R_{gb})}$$

5-h

Since the resistance of grains *Rg* is small relative to that of grain boundaries *Rgb* (Rgb>>Rg) and also grain boundary capacitances C$_{gb}$ is greater than grain capacitances C$_g$ (Čgb~10Cg) [35-36], so equations (5-g) and (5-h) can be simplified to $\varepsilon_s \approx \frac{c_{gb}}{C_o}$ and $\tau \approx R_g c_{gb}$ respectively, the values of R$_g$ and C$_g$ were calculated and listed in Table 4.

TABLE 4 . The Dielectric constant at low frequency(ε_s) and high frequency (ε_∞) and The relaxation time τ(sec) as a function of La^{3+} content for CoAl$_{2-x}$La$_x$O$_4$.

X (content)	s	τ(sec) x 10^{-7}	ε_s	ε_∞	R$_g$	C$_g$ X 10^{-12}
0	0.3315	13.025	130.25	52.32	56706.247	1.153
0.04	0.4915	7.446	145.21	114.96	48805.217	1.285
0.08	0.439	7.681	107.53	92.53	66434.751	0.9516
0.10	0.0736	9.011	177.52	155.21	46053.217	1.571
0.12	0.3635	8.656	120.32	97.87	66498.753	1.065

By analyzing the calculated values of *s* in Table 4, for values we are observed that values of *s* for all the samples less than unity suggest the dominance of ac conduction phenomenon in the prepared samples. The relaxation time τ (sec) for all La^{3+} cations substituted cobalt aluminates nanoparticles, were greater than for CoAl$_2$O$_4$ sample which confirmed the effects of La^{3+} ion substitution on the structural of CoAl$_{2-x}$La$_x$O$_4$.

Analyze of the grain boundary and electrode effect results is clearly observed in the complex impedance (*Z'* vs *Z''* plot or complex impedance plane) plots as shown in Fig. 9 (a). The dielectric structure is an inhomogeneous medium consisting of well conducting grains separated by poor conducting grain boundaries of higher permittivity , which indicates the ionic conductivity emerges from the inter-grain hopping mechanism. At lower frequency, the grain boundaries are more effective than the grains, giving rise to higher value of dielectric constant [31].

Many factors may lead to non-Debye relaxation such as grain boundaries, grain orientation, grain size distribution and defect distribution [34-35]. The peak intensities in *Z''* arising from the grains are very weak due to the small resistance of grains relative to that of grain boundaries *(Rgb>>Rg*) and also grain boundary capacitances *Cgb* is greater than grain capacitances *Cg (Cgb~10Cg)* [35-36], as shown in Figure 9 (b). The grain effects will be magnified in the electric modulus formalism (*M*=M'+iM''*). The Complex electric modulus plane plot (*M'* vs *M''*) is used together with the complex impedance plane (*Z'* vs *Z''* plot) to separate grain and grain-boundary effects and/or to distinguish the microscopic processes responsible for localized dielectric relaxations and long-range conductions [36].

Conclusions

A series of La^{3+} cations substituted cobalt aluminates nanoparticles with an average size in the range of 13-58 nm were successfully synthesized by using a simple co-precipitation method. The crystal structures of all cobalt aluminates CoAl$_{2-x}$La$_x$O$_4$ (0.0 ≤ x ≤ 0.12) nanoparticles samples are cubic spinel. The substitution of La^{3+} cations in cobalt aluminates have significant impact on the change and development of crystal structure, morphologies, dielectric, optical and magnetic properties. The XRD analysis confirmed the single-phase cubic spinel structure. The variation of lattice parameter (*a*) and crystallite size (*D*) with La^{3+} content for CoAl$_{2-x}$La$_x$O$_4$ nanoparticles is linear. The increase of lattice parameter with La^{3+} content, obeying Vegard's law. The magnetic ions in cobalt aluminates nanoparticles substituted with La^{3+} cations far to each other and the hopping length increase, due to the larger ionic radius of La^{3+}(0.615 A°) than that of Al^{3+} (0.53 A°). There is a high degree of agreement for values of the crystallite size of CoAl$_{2-x}$La$_x$O$_4$ (0.0 ≤ x ≤ 0.12) nanoparticles which calculated from Scherrer formula and Williamson–Hall method and that from TEM. By analyzing TEM images, we have demonstrated the formation of spherical nanoparticles, homogeneous in shape and size. The results of the FTIR spectra showed that there are two main absorption bands which are characteristic of spinel aluminate in the wavelength range 550-700 cm^{-1}. The optical properties of CoAl$_{2-x}$La$_x$O$_4$ nanoparticles have been investigated. Absorption band edge wavelength λ_g (nm), indirect optical band gap and Urbach energy DE$_u$ of CoAl$_{2-x}$La$_x$O$_4$ nanoparticles decrease with the increase La^{3+} content ,while the refractive index values increase which confirms the enhancement of density of the CoAl$_2$O$_4$ nanoparticles with rising La^{3+} content.

The results from magnetic hysteresis (M-H) loop showed that in $CoAl_{2-x}La_xO_4$ nanoparticles, some of Li^{3+} cations occupy the tetrahedral (A) sites, which switch on the A–B superexchange interaction and give rise to a ferromagnetic behavior. The addition of La^{3+} content enhances the dielectric properties. The relaxation time Ⴀ (sec) for all La^{3+} cations substituted cobalt aluminates nanoparticles, were greater than for $CoAl_2O_4$ sample which confirmed the effects of La^{3+} ion. The values of *s* for all the samples less than unity suggest the dominance of ac conduction phenomenon in the prepared samples. In general the optical, magnetic, and dielectric properties of cobalt aluminates have improved, due to the addition of La^{3+} content, which give it a wider scope for use as catalysis, ceramics, magnetic materials, and humidity sensor
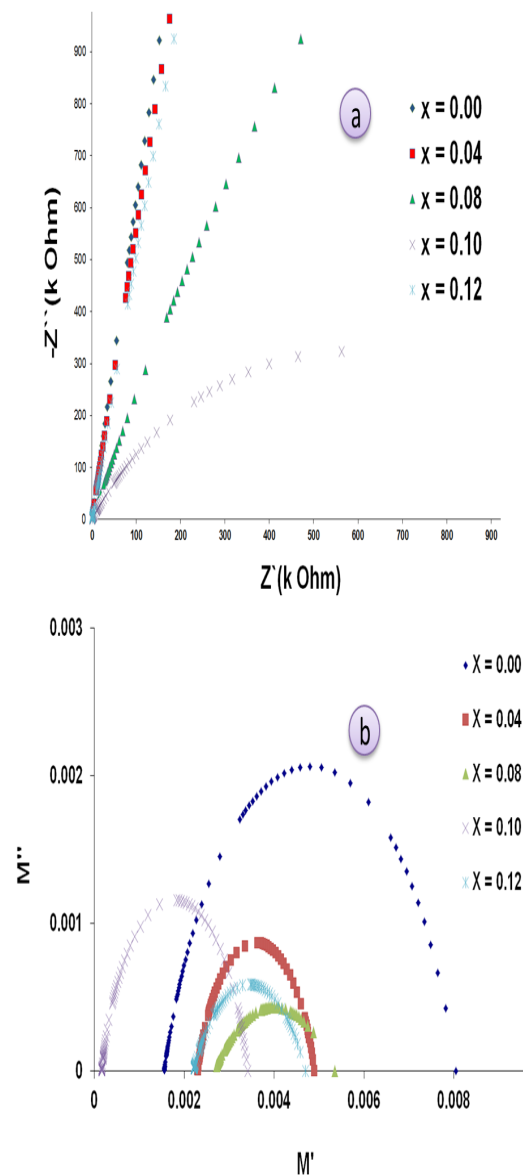
Fig. 9. (a) complex impedance plane(*Z′* vs *Z″* plot) and (b) Complex electric modulus plane plot (*M′* vs *M″*).

References

1. Ragupathi C, Vijaya JJ, Kennedy LJ and Bououdina M. Nanostructured copper aluminate spinels: synthesis, structural, optical, magnetic, and catalytic properties. *Materials Science in Semiconductor Processing,* **24**:46-156 (2014).

2. Huang YH, Wang SF, Tsai AP and Kameoka S. Reduction behavior sand catalytic properties form ethanol steam reforming of Cu-based spinel compounds CuXO (X = Fe, Mn, Al, La). *Ceramics International,* **40** (3),4541-4551(2014).

3. Yanagiya S, Van Nong N, Xu J and Pryds N. The effect of (Ag, Ni, Zn)-addition on the thermoelectric properties of copper aluminate. *Materials (Basel),* 3 (1):318-328(2010).

4. C. Maurizio, N. El Habra, G. Rossetto, M. Merlini, E. Cattaruzza, L. Pandolfo, M. Casarin,XAS and GIXRD Study of Co Sites in $CoAl_2O_4$ Layers Grown by MOCVD, *Chem.Mater.* **22** (2010)

5. Gherbi R, Nasrallah N, Amrane A, Maachi R and Trari M. Photocatalytic reduction of Cr(VI) on the new hetero-system $CuAl_2O/TiO_2$. *Journal of Hazardous Materials,* **186** (2-3):1124-1130 (2011).

6. Arjmand M, Azad AM, Leion H, Mattisson T and Lyngfelt A. Evaluation of $CuAl_2O_4$ as an oxygen carrier in chemical-looping combustion. *Industrial & Engineering Chemistry Research,* **51** (43):13924-13934 (2012).

7. Gaudon M, Robertson LC, Lataste E, Duttine M, Ménétrier M and Demourgues A. Cobalt and nickel aluminate spinels: blue and cyan pigments. *Ceramics International*, **40** (4):5201-5207(2014).

8. Torkian L and Daghighi M. Effects of ⬚-alanine on morphology and optical properties of CoAlO nanopowders as a blue pigment. *Advanced Powder Technology,* **25** (2):739-744 (2014).

9. Chandradass J, Balasubramanian M and Kim KH. Size effect on the magnetic property of $CoAl_2O_4$nanopowders prepared by reverse micelle processing. *Journal of Alloys and Compounds,* **506** (1):395-399(2010).

10. Duan X, Pan M, Yu F and Yuan D. Synthesis, structure and optical properties of CoAlO spinel nanocrystals. *Journal of Alloys and Compounds*, **509** (3):1079-1083(2011).

11. Thormählen P, Fridell E, Cruise N, Skoglundh M and Palmqvist A. The influence of CO_2, C_3H, NO, H, HO or SO. on the low-temperature oxidation of CO on a cobalt-aluminate spinel catalyst $(Co_{1.66}Al_{1.34}O_4)$ *Applied Catalysis B: Environmental*, **31** (1):1-12 (2001).

12. M.J. Akhtar, M. Nadeem, S. Javaid, M. Atif, Cation distribution in nanocrystalline $ZnFe_2O_4$ investigated using x-ray absorption fine structure spectroscopy, *J. Phys. Condens. Matter.* **21**, 405303 (2009).

13. A.I. Borhan, A.R. Iordan, M.N. Palamaru, Correlation between structural, magnetic and electrical properties of nanocrystalline Al^{3+} substituted zinc ferrite, Mater. Res. Bull. 48, 2549-2556(2013).

14. ment *via* polyacrylamide gel method Powder Technology, 266:236-239 (2014).

15. Li W, Li J and Guo J. Synthesis and characterization of nanocrystalline $CoAl_2O_4$ spinel powder by low temperature combustion. *Journal of the European Ceramic Society*, **23** (13):2289-2295 (2003).

16. Mindru I, Marinescu G, Gingasu D, Patron L, Ghica C and Giurginca M. Blue $CoAl_2O$ spinel via complexation method. *Materials Chemistry and Physics*, **122** (2-3):491-497 (2010).

17. Tsai WC, Liou YH and Liou YC. Microwave dielectric properties of $MgAl_2O_4$–CoAlO spinel compounds prepared by reaction-sintering process. *Materials Science and Engineering B*, 177(13):1133-1137 (2012).

18. Yu F, Yang J, Ma J, Du J and Zhou Y. Preparation of nanosized $CoAl_2O$ powders by sol–gel and sol–gel-hydrothermal methods. *Journal of Alloys and Compounds,* **468** (1-2):443-446(2009).

19. D. El-Said Bakeer, & A.H. Sakr,Structural, Optical, Magnetic, and Dielectric Properties of Cr^{3+} Substituted Cobalt Aluminate Nanoparticles, *J Supercond Nov Magn,* **32** : 2119–2132 (2019).

20. P. Hu, D. Pan, X. Wang, J. Tian, J. Wang, S. Zhang, A. Volinsky, Fuel additives and heat treatment effects on nanocrystalline zinc ferrite phase composition, *J. Magn. Magn. Mater.* **323**, 569-573 (2011).

21. D. EL-Said Bakeer, A. I. Abou-Aly, N. H. Mohammed, R. Awad, M. Hasebbo, :Characterization and Magnetic Properties of Nanoferrite $ZnFe_{2-x}La_xO_4$ Prepared by Co-Precipitation Method, *J Supercond Nov Magn.* **30**, 893–902 (2017).

22. M. Ishaque, M.U. Islam, M. Azhar Khan, I.Z.

Rahman, A. Genson, ampshire, S.,Structural, electrical and dielectric properties of yttrium substituted nickel ferrites, *Physica* B 405, 1532-1540 (2010).

23. K. Venkateswarlu, A.C. Bose, N. Rameshbabu, X-ray peak broadening studies of nanocrystalline hydroxyapatite by Williamson–Hall analysis, *Physica B: Condensed Matter,* 405, 4256-4261(2010).

24. S. Suguna, , S. Shankar, S. K. Jaganathan, A. Manikandan,Novel Synthesis of Spinel $Mn_xCo_{1-x}Al_2O_4$ (x = 0.0 to 1.0) Nanocatalysts: Effect of Mn^{2+} Doping on Structural, Morphological, and Opto-Magnetic Properties, *J Supercond Nov Magn.* **30**, 691–699(2017).

25. M. Khairy, Effect of Ni content on optical, colorimetric, surface and magnetic properties of $Ni_xCo_{1-x}Al_2O_4$ nanoparticles, *J. IRAN. CHEM. SOC.***13**, 671–677(2016).

26. D. Visinescu, C. Paraschiv, A. Ianculescu, B. Jurca, O. Vasile, B. Carp, The environmentally benign synthesis of nanosized $Co_xZn_{1-x}Al_2O_4$ blue pigments, *Dyes Pigm.* **87**, 125-131(2010).

27. M.Y. Nassar, Size-controlled synthesis of $CoCO_3$ and Co_3O_4 nanoparticles by free-surfactant hydrothermal method, *Mater. Lett.* **94**, 112–115(2013).

28. K. Dutta, SK .De, Optical and electrical characterization of polyaniline-silicon dioxide Nanocomposite ,*Phys. Lett.* A, 361,141-145(2007).

29. S. F. Oboudi, M.T. Abdul Nabi, W.A. Al-Taa'y, R. M. Yusop, D. Derawi, E. Yousif,Dispersion Characterization of conductive polymer, *Int. J. Electrochem. Sci.,* **10**, 1555 – 1562(2015).

30. D. Xue, G. Chai, X. Li, X. Fan, Effects of grain size distribution on coactivity and permeability of ferromagnets, *J. Magn. Magn. Mater.* **320**, 1541–1543(2008).

31. A. K. Jonscher, Dielectric Relaxation in Solids, London: Chelsea Dielectric Press, Chap. 2, pp. 13-61(1983).

32. M. Graca, MA .Valente, MG. Ferreira da Silva, *Journal of Non-Crystalline Solids;* 325(1–3), 267-274 (2003).

33. Sahoo S, Mahapatra P K, Choudhary R N P and Nandagoswamy M L, Dielectric and impedance spectroscopy of (Ba, Sm)(Ti, Fe)O3 system in the low-medium frequency range *J. Mater. Sci: Mater. Electron.* **26** 6572–84 (2015).

34. B. Dhanalakshmi, P.pKollu, B.ParvatheeswaraRao, P.S.V.SubbaRao. *Ceramics International, 42* (2), 2186–2197(2016).

35. R. Nongjai, S. Khan, K. Asokan, H. Ahmed, and I. Khan, *Journal of Applied Physics,* **112** (8),084321(2012) .

36. Jianjun Liu, Chun-Gang Duan, Wei-Guo Yin, Wai-Ning Mei, R. W. Smith, and John R. Hardy, Large Dielectric Constant and Maxwell-Wagner Relaxation in $Bi_{2/3}Cu_3Ti_4O_{12}$ *Phys. Rev. B* 70, 144106 (2004).

تأثير اللانثانوم على الخصائص الفيزيائية والبصرية والمغناطيسية والعزل الكهربي لجسيمات $CoAl_{2-x}La_xO_4$ النانوية

عبدالحميد عبدالونيس صقر

قسم الفيزياء –كلية العلوم –جامعة دمنهور .

في هذه الدراسة تم التحقق من تأثير اضافة أيون اللانثانوم La^{3+} على الخصائص التركيبية والبصرية والمغناطيسية وخصائص العزل الكهربي لجسيمات نانوية من ألومينات الكوبالت $(CoAl_{2-x}La_xO_4)$ في سلسلة $(0.12 \leq x \leq 0.00)$. حيث تم تحضير الجسيمات النانوية بطريقة الترسيب المشترك. واستخدامت تقنية حيود الأشعة السينية (XRD) للتحقق من بنية ألومينات الإسبنيل المكعبة. وقد لوحظ انه مع زيادة محتوي ايون La^{3+} فان ثابت الشبيكة البلورية (a) يزيد من ٨.٠٧٨ الي ٩.٩٨٣ والكثافة النظرية للأشعة السينية (ρ_{x-ray}) تزداد من ٤.٤٨٩ الي ٤.٥٣٢ . وقد اوضحت نتائج صور الميكروسكوب الالكتروني النافذ TEM تشكيلا كروي متجانسا للجسيمات النانوية. كما أشار تحليل أطياف الاشعه تحت الحمراء FTIR إلى وجود نطاقي امتصاص رئيسيين (تراوح طول الموجة ٧٠٠-٥٥٠ سم $^{-1}$) . والذي يُنسب إلى ألومينات الإسبنيل. من نتائج أطياف الامتصاص البصري في نطاق الاشعه فوق البنفسجة و الضوء المرئي . ومن دراسة الخواص الضوئية للجسيمات النانوية مع زيادة المحتوي من La^{3+} أظهرت زيادة في فجوة النطاق البصري E^{opt} من ١.٠١ الي ١.٦٠ (eV) و زيادة معامل الانكسار من ٤.٩٨٣ الي ٢.٩٣٠ . بدراسة الخواص المغناطيسية اظهرت النتائج زيادة في سلوك المغنطيسية الحديدية (superparamagnetic) مع زيادة محتوى La^{+3} . والذي قد يكون ناتجًا عن تكوين جسيم أحادي المجال بحجم الجسيمات الصغيرة . وقد أظهرت الدراسة أن قيمة الممانعة وعامل الفقد   تتغير وتتحسن بزيادة المحتوي من ايون La^{3+} وكذلك ثابت العزل بجزأيه الحقيقي والخيالي. وعليه فان إضافة ايونات La^{3+} للجسيمات النانوية $CoAl_{2-x}La_xO_4$ أدت الي تعزيز الخصائص الضوئية , العازلة الكهربي والمغناطيسية الحديدة عنها في العينات الاصلية غير المضاف لها .